Hardware-Efficient Microwave-Activated Tunable Coupling between Superconducting Qubits

Bradley K. Mitchell, Ravi K. Naik, Alexis Morvan, Akel Hashim, John Mark Kreikebaum, Brian Marinelli, Wim Lavrijsen, Kasra Nowrouzi, David I. Santiago, and Irfan Siddiqi

Phys. Rev. Lett. **127**, 200502 — Published 9 November 2021

DOI: 10.1103/PhysRevLett.127.200502

Hardware-Efficient Microwave-Activated Tunable Coupling Between Superconducting Qubits

Bradley K. Mitchell,[1,2,*] Ravi K. Naik,[1,2,*] Alexis Morvan,[1,2] Akel Hashim,[1,2] John Mark Kreikebaum,[1,3] Brian Marinelli,[1,2] Wim Lavrijsen,[2] Kasra Nowrouzi,[1,2] David I. Santiago,[1,2] and Irfan Siddiqi[1,2,3]

[1] *Quantum Nanoelectronics Laboratory, University of California, Berkeley, Berkeley CA 94720*
[2] *Computational Research Division, Lawrence Berkeley National Laboratory, Berkeley CA 94720*
[3] *Materials Science Division, Lawrence Berkeley National Laboratory, Berkeley CA 94720*

(Dated: August 2, 2021)

Generating high-fidelity, tunable entanglement between qubits is crucial for realizing gate-based quantum computation. In superconducting circuits, tunable interactions are often implemented using flux-tunable qubits or coupling elements, adding control complexity and noise sources. Here, we realize a tunable ZZ interaction between two transmon qubits with fixed frequencies and fixed coupling, induced by driving both transmons off-resonantly. We show tunable coupling over one order of magnitude larger than the static coupling, and change the sign of the interaction, enabling cancellation of the idle coupling. Further, this interaction is amenable to large quantum processors: the drive frequency can be flexibly chosen to avoid spurious transitions, and because both transmons are driven, it is resilient to microwave crosstalk. We apply this interaction to implement a controlled phase (CZ) gate with a gate fidelity of 99.43(1)% as measured by cycle benchmarking, and we find the fidelity is limited by incoherent errors.

High-fidelity two-qubit gates are critical for building quantum computers that can outperform classical computers [1]. Important qualities for entangling schemes include high fidelity, low leakage [2], an ability to couple and decouple qubits, and minimal hardware resources. In circuit QED [3], two-qubit gates with errors below the 1% threshold for surface code-based quantum error correction [4] have been demonstrated. Approaches utilizing qubits and/or couplers with flux-tunable transition frequencies have shown high tunability [5, 6], full decoupling of qubits [7], and gate fidelities above 99.8% [8–10]. However, these approaches require additional control circuitry, and introduce decoherence channels.

A scheme with reduced hardware complexity while retaining the above capabilities would simplify the scaling of high-fidelity two-qubit gates to many-qubit processors. Charge-activated two-qubit gate schemes [11–17] do not require additional control circuitry, and they are compatible with fixed-frequency qubits. Particularly, the cross resonance (CR) gate [15] has demonstrated a gate fidelity as high as 99.7% [18]. However, this scheme has residual idle ZZ coupling between qubits [19] due to interactions between their noncomputational transitions. This idle coupling causes correlated errors, dephasing, and spectator errors [20–23]. Mitigating idle ZZ coupling without a flux-tunable coupler was done using dynamical decoupling [16, 24, 25] and using opposite-anharmonicity qubits [26], with added overhead in circuit depth and in hardware complexity, respectively. Recently, cancellation of the ZZ coupling between capacitively-coupled fluxonium qubits was also reported [27].

In this Letter, we demonstrate a tunable, charge-activated ZZ interaction between two fixed-frequency transmon qubits [28] with fixed coupling. We show full cancellation of ZZ coupling between the qubits, and realize a CZ gate with a fidelity of 99.43(1)%. The interaction is realized by driving the transmons simultaneously at a frequency between the $|0\rangle \rightarrow |1\rangle$ and $|1\rangle \rightarrow |2\rangle$ transitions, generating a conditional Stark shift. In contrast to the CR interaction, here the drive frequency can be tuned to avoid driving unwanted transitions, making this interaction suitable for use on large devices with crowded frequency spectra [29, 30]. Further, *in situ* control over the coupling enables controlled phase gates with arbitrary phase angles $\mathrm{CZ}\,(\phi)$, which are useful for noisy intermediate-scale quantum (NISQ) algorithms [31–33].

Consider two coupled, simultaneously driven transmons, as illustrated in Figure 1. The Hamiltonian of the two transmons, in the frame of the drive at frequency ω_d and making the Duffing approximation of the transmon [28], is given by

$$H_\mathrm{qb} = \sum_{i=\mathrm{c,t}} \left(\omega_i - \omega_\mathrm{d}\right) a_i^\dagger a_i + \frac{\eta_i}{2} a_i^\dagger a_i^\dagger a_i a_i, \qquad (1)$$

where for transmon i, a_i is the bosonic annihilation operator, ω_i is the transition frequency between $|0\rangle$ and $|1\rangle$, η_i is the anharmonicity, and $\hbar = 1$. Each drive term is given by $H_{\varepsilon_i} = \left(\varepsilon_i a_i + \varepsilon_i^* a_i^\dagger\right)$, where ε_i is the complex drive amplitude, and the coupling term with strength J is $H_J = J\left(a_\mathrm{c}^\dagger a_\mathrm{t} + a_\mathrm{c} a_\mathrm{t}^\dagger\right)$, where we denote the higher frequency transmon Q_c, and the lower frequency transmon as Q_t. The total Hamiltonian is $H = H_\mathrm{qb} + H_J + H_{\varepsilon_\mathrm{c}} + H_{\varepsilon_\mathrm{t}}$.

The Stark-induced ZZ interaction can be understood through the lens of the CR effect: when driving the control qubit with amplitude ε_c at the target qubit frequency

* These two authors contributed equally. Correspondence should be addressed to bradmitchell@berkeley.edu and rnaik24@berkeley.edu

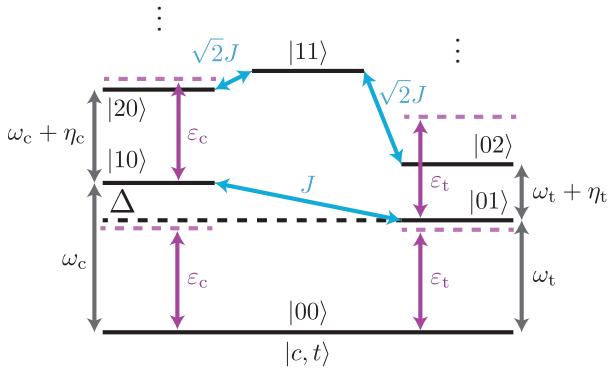

FIG. 1. **Drive scheme for the Stark-induced ZZ interaction**. Transmons are detuned by $\Delta = \omega_c - \omega_t$ indicated by the black dashed line, and coupled via exchange coupling J. They are driven simultaneously with amplitudes ε_c, ε_t between frequencies ω_t and $\omega_c+\eta_c$, indicated with purple dashed lines. The simultaneous driving introduces conditional Stark shifts, i.e., a ZZ interaction.

ω_t, the target experiences a drive amplitude $\tilde{\varepsilon}_n$ that depends on the control state $|n\rangle$ [15, 34]. In the qubit subspace, the CR drive realizes an entangling ZX interaction with rate $\mu = (\tilde{\varepsilon}_0 - \tilde{\varepsilon}_1)/2$. In the limit $\varepsilon_c/\Delta_t \ll 1$, detuning the drive frequency from the target qubit frequency $\Delta_t = \omega_t - \omega_d$ results in a conditional Stark shift of the target qubit frequency $\tilde{\delta}_n$, where

$$\tilde{\delta}_n = \frac{\tilde{\varepsilon}_n^2}{\Delta_t}. \tag{2}$$

The drive-induced ZZ interaction ζ then is given by $\zeta = \tilde{\delta}_0 - \tilde{\delta}_1$, which can be expressed in terms of μ as

$$\zeta = 2\mu\,(\tilde{\varepsilon}_0 + \tilde{\varepsilon}_1)\,/\Delta_t. \tag{3}$$

This conditional Stark shift is much smaller than the CR rate $\zeta \ll \mu$. However, applying a drive simultaneously to the target qubit at amplitude ε_t modifies the total drive amplitude on the target to $\tilde{\varepsilon}_n + \varepsilon_t$. Replacing $\tilde{\varepsilon}_n \to \tilde{\varepsilon}_n + \varepsilon_t$ above, ζ then scales linearly to first order with ε_t

$$\zeta = \frac{2\mu}{\Delta_t}\,(\tilde{\varepsilon}_0 + \tilde{\varepsilon}_1 + 2\varepsilon_t) + O(|\varepsilon_t|^2). \tag{4}$$

By driving both transmons simultaneously, one can generate a ZZ coupling between transmons with detuning Δ suitable for the CR gate, with interaction rates comparable to the CR effect. Note that the qubits are interchangeable and this can be generalized to systems that are not transmons [27]. See the supplement for a perturbation theory derivation.

We next experimentally investigate how the Stark-induced ZZ interaction depends on the field amplitudes on each qubit ε_c, ε_t and the frequency of the drive field ω_d. We measure ζ using Ramsey interferometry [35] and extract the frequency shift of Q_t conditioned on the state Q_c being $|0\rangle$ or $|1\rangle$ when applying the drive. We find agreement between our measurements and numerical simulations when microwave crosstalk is included.

We show in Figure 2 experiments measuring ZZ as a function of drive parameters. The experiments were performed on a pair of fixed-frequency, fixed-coupling transmons on a device of the same design as in [36], with parameters $\omega_c/2\pi = 5.845\,\text{GHz}$ ($\omega_t/2\pi = 5.690\,\text{GHz}$), $\eta_c/2\pi = -244.1\,\text{MHz}$ ($\eta_t/2\pi = -247.1\,\text{MHz}$) with static ZZ coupling $\zeta_0/2\pi = 307\,\text{kHz}$, corresponding to an inferred exchange coupling strength $J = 3.45\,\text{MHz}$.

In the presence of microwave crosstalk, ε_c and ε_t are complex linear combinations of CZ drive amplitudes A_c and A_t applied to the control and target transmon drive lines, as shown in Figure 2 (a). This is expressed via the crosstalk matrix

$$\begin{pmatrix}\varepsilon_c\\ \varepsilon_t\end{pmatrix} = \begin{pmatrix} e^{i\theta_c} & C_{ct}e^{i\varphi_{ct}} \\ C_{tc}e^{i\varphi_{tc}} & 1\end{pmatrix}\begin{pmatrix}A_c\\ A_t e^{-i\varphi_d}\end{pmatrix}, \tag{5}$$

where C_{ct} (φ_{ct}) denotes the crosstalk amplitude (phase). The phase θ_c results from electrical delay between the drive lines. For these experiments in Figure 2 (b), we set $\Delta_t = 40\,\text{MHz}$ and measured the ZZ interaction while varying drive phase φ_d and global drive amplitude A, where $A_c = A_t = A$. The experimental data deviates from the crosstalk-free simulations, which diagonalize the full system Hamiltonian (see supplementary material). This is remedied by including the crosstalk matrix parameters in the model fit. With no crosstalk, ζ is symmetric about ζ_0 between in-phase and out-of-phase driving. Additionally, in Fig. 2 (c) we varied A_t and A_c independently while keeping φ_d fixed to $\varphi_d = 1.31\,\text{rad}$. The linear dependence of ζ on the drive amplitude is observed for non-zero A_c amplitudes, as predicted in the theoretical description. Note that the predicted linear dependence is valid only when the drive amplitude is weak compared to the drive detuning from the transmon transition frequencies. These experiments demonstrate tunability of the sign of the ZZ coupling, with magnitude $\zeta \approx 0$, to one order of magnitude larger than ζ_0, by adjusting the relative phase between the drives. This flexibility is well-captured by numerical simulation, and is resilient to microwave crosstalk,

Using the strong ZZ interactions, we next calibrate a CZ gate, which is realized from Hamiltonian terms IZ, ZI, and ZZ: $\text{CZ} = \exp\left(-\frac{i}{2}\frac{\pi}{2}\left(-ZI - IZ + ZZ\right)\right)$. We first calibrate the entangling term ZZ, and then correct local phase errors on the each qubit using virtual Z gates [37]. To calibrate the ZZ term, we prepare the target qubit in superposition, apply the CZ pulse, and measure the target qubit Bloch vector r_0 (r_1) when the control qubit is in the $|0\rangle$ ($|1\rangle$) state (see Fig. 3 (a)). To maximize entanglement, we maximize the quantity

$$R = \frac{1}{2}||r_0 - r_1||^2, \tag{6}$$

which measures the normalized vector distance between target Bloch vectors conditioned on the control qubit

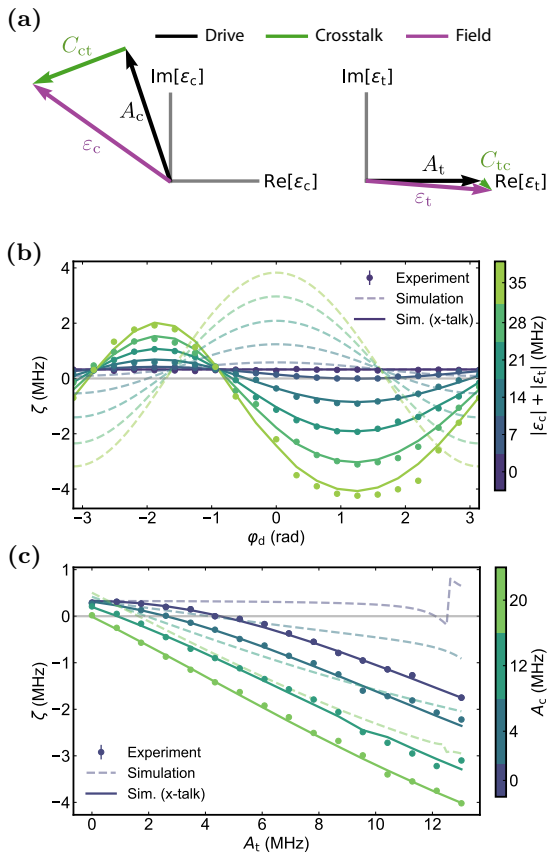

FIG. 2. ZZ **as a function of drive parameters, crosstalk** **(a)** The control and target drive fields ε_c, ε_t are complex combinations of the drive line amplitudes A_c, A_t, mixed via the microwave crosstalk matrix C. **(b)** ZZ versus relative drive phase φ_d, for several overall drive amplitudes $|A| = |A_c| = |A_t|$. Field amplitudes indicated in the colorbar are determined by fitting the data (dots) to numerical simulations including crosstalk (solid lines). Microwave crosstalk affects both the relative magnitude of ZZ between positive and negative signs, and the phase corresponding to maximal $|\zeta|$. With no crosstalk (dashed lines) the predicted ζ is symmetric about $\varphi_d = 0$ and ζ_0. Error bars indicate Ramsey frequency fit uncertainty. **(c)** ZZ versus target drive amplitude A_t for several control drive amplitudes A_c (colorbar). Linear behavior with respect to drive amplitude is observed when driving both transmons, as predicted. As drive strength approaches the drive detunings from the transmon transitions, this linear dependence is predicted to break down (see supplementary material).

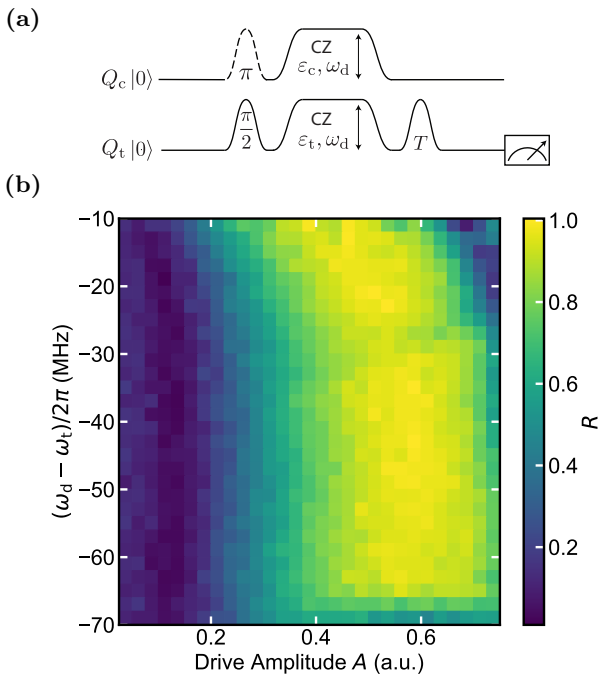

FIG. 3. **CZ Gate Calibration (a)** Pulse sequence for calibrating the amplitude and frequency of the CZ pulse. The target is prepared in superposition, followed by the CZ pulse, and then tomographic pulses T are applied to measure the target qubit Bloch vector r_i for each control qubit state $|i\rangle \in \{0, 1\}$. The global pulse amplitude and frequency are calibrated by selecting parameters that maximize entanglement measure R. **(b)** R as a function of the CZ gate amplitude A and drive detuning from the target $(\omega_d - \omega_t)$. There is a band of frequencies where R is maximal to realize the CZ gate. There is also a pulse amplitude around $A = 0.1$ where R is minimal, corresponding to ZZ cancellation.

state [24]. For the drive pulse, we use a cosine ramp with a flat top, with the flat top of the pulse set to 40% of the total pulse time. The parameters to calibrate include pulse time τ_p, drive frequency ω_d, drive amplitudes A_c and A_t, and relative phase φ_d. Pulse time is determined by experiments sweeping drive amplitudes and relative phase, like those shown in Figure 2.

We calibrate the gate on a separate qubit pair than was used for the preceding experiments, with parameters $\omega_c/2\pi = 5.4696\,\text{GHz}$ $(\omega_t/2\pi = 5.315\,\text{GHz})$, $\eta_c/2\pi = -270.5\,\text{MHz}$ $(\eta_t/2\pi = -273.0\,\text{MHz})$ with static ZZ coupling $\zeta_0/2\pi = 170\,\text{kHz}$, corresponding to an inferred exchange coupling strength $J = 2.79\,\text{MHz}$. We set $\tau_p = 201\,\text{ns}$, and pulse amplitudes A_c, A_t and relative phase φ_d are selected to maximize $|\zeta|$.

To calibrate the drive frequency ω_d and overall pulse amplitude A, we find the values that maximize R. In Figure 3 (b), one observes a bandwidth of 40 MHz where maximal R is achievable. There is also a region around $A = 0.1$ where R is approximately zero, corresponding to ZZ interaction cancellation. To map the pulse to a CZ gate, local phase corrections are calibrated by measuring the individual qubit Pauli Z error using Ramsey-type experiments.

To assess gate performance, we perform randomized benchmarking (RB) [38, 39] experiments. We first perform Interleaved Randomized Benchmarking (IRB) [40], shown in Figure 4 (a). The IRB protocol interleaves a gate of interest between a sequence of randomly chosen Clifford gates, also called Clifford twirling, which randomizes gate errors to a depolarizing channel. The

sequence fidelity is measured with increasing sequence length m and the decay parameter p is extracted by fitting to the exponential model $P(m) = A \cdot p^m$ [41]. Because IRB estimates F_{CZ} using exponential decays, it is insensitive to state preparation and measurement (SPAM) errors. The decay parameter for the interleaved experiment $p_{IRB} = 0.9672(7)$ and the reference experiment $p_{RB} = 0.9744(9)$ give an estimate of the CZ gate fidelity $F_{CZ} = 1 - \frac{d-1}{d}(1 - p_{IRB}/p_{RB}) = 99.44(9)\%$, where $d = 2^n$ for n qubits (here $d = 4$). The upper- and lower-bounds on gate fidelity estimates from IRB have been shown to span orders of magnitude [42]. When p_{RB} is comparable to p_{IRB}, the IRB F_{CZ} estimate uncertainty increases. From these IRB results, the upper- and lower-bounds on F_{CZ} are between 91.9(2)% and 99.96(1)%, spanning nearly 2 orders of magnitude in gate error (1-F_{CZ}).

To reduce gate fidelity estimate uncertainty, we run the cycle benchmarking (CB) protocol [43], shown in Figure 4 (b). The CB protocol is similar to IRB, in that the gate, or cycle, of interest is interleaved between randomly chosen gates. Instead of Clifford gates, in CB the cycle is twirled with multi-qubit Pauli gates, which are tensor products of single-qubit Pauli gates. Pauli twirling maps gate errors into stochastic Pauli errors, which are measured by preparing each eigenstate of the multi-qubit Pauli basis, e.g. XX or YZ for two-qubit CB, and fitting the sequence fidelity to an exponential decay parameter (e.g., p_{XX}, p_{YZ}) as a function of CB sequence length. The error rate $e_i = 1 - p_i$ for Pauli eigenstate i measures errors in the cycle that do not commute with that Pauli operator. We performed CB with cycle lengths of $m \in \{2, 16, 32\}$ for the CZ cycle, and for the empty cycle to estimate the fidelity of the Pauli twirling gates, and extracted the error rate of each Pauli term, which is plotted in Figure 4 (b). Averaging over all Pauli preparations, we extract average Pauli decay parameters for both cycles $p_{CZ} = 0.98937(8)$ and $p_I = 0.99702(3)$. We then estimate the CZ gate fidelity as in the IRB protocol, to be $F_{CZ} = 1 - \frac{d-1}{d}(1 - p_{CZ}/p_I) = 99.43(1)\%$, with a worst-case (best-case) fidelity bound of 97.52(2)% (99.764(5)%). Note that the interval between these bounds from CB are narrower than that of IRB, because the fidelity of the Pauli twirling operation is higher than Clifford twirling.

To understand how to reduce the CZ gate error, it is important to distinguish the different error sources. Different error types include coherent errors, such as miscalibration, stochastic errors, such as dephasing errors, and leakage errors, involving population transfer to non-computational states of the system. We measure the leakage-per-gate using leakage randomized benchmarking (LRB) [44, 45], realized by extracting $|2\rangle$-state outcomes for Q_c and Q_t in IRB experiments. We fit the qubit $|2\rangle$-state population data shown in Figure 4 (c) to an exponential model [44, 45] for both reference RB and interleaved RB experiments. We resolve the leakage-per-gate for each transmon to be 0.014% and 0.007% for Q_c and Q_t respectively, indicating leakage is not a dominant source of errors for this gate.

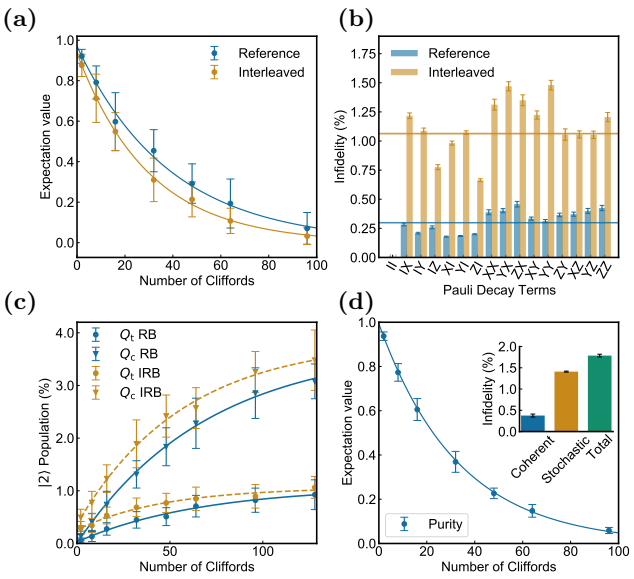

FIG. 4. **Benchmarking Results (a)** Interleaved RB. Exponential decay of Clifford sequence fidelity (y-axis) for different Clifford sequence lengths with (gold) and without (blue) the interleaved CZ gate. From reference and interleaved decay parameters $p_{RB} = 0.9744(9)$ and $p_{IRB} = 0.9672(7)$, respectively, we extract a CZ gate fidelity of 99.44(9)%. **(b)** Cycle Benchmarking results. The error rate e_i is obtained for the prepared Pauli eigenstate i from the exponential decay of sequence fidelity p_i with increasing sequence length. A larger error rate for a given Pauli eigenstate indicates errors in the cycle that do not commute with the compiled Pauli term. The process infidelity is the error averaged across Pauli terms. By performing CB for the CZ gate (gold) and the identity cycle (blue), we extract a gate fidelity of 99.43(1)%. **(c)** Leakage Randomized Benchmarking. By monitoring the $|2\rangle$ state of each transmon when running an IRB experiment, the reference and interleaved $|2\rangle$ state population data are fit to an exponential model to extract the leakage-per-gate for each transmon. **(d)** Purity Benchmarking distinguishes coherent from stochastic errors by measuring the decay of the purity (main plot) of the two-qubit density matrix by performing state tomography for each random Clifford RB sequence, and comparing the purity decay to the RB decay. Inset: breakdown of Clifford process infidelity between coherent and stochastic contributions. We find stochastic error to be the dominant source of error.

To distinguish coherent and stochastic error sources, we perform purity benchmarking [46, 47], which measures the decay of the purity of the two-qubit density matrix by performing state tomography after Clifford RB sequences. Figure 4 (d) shows the purity decay curve, and the inset shows the breakdown of the Clifford process infidelity $e_F = (1 - p_{RB})\left(1 - 1/d^2\right) = 1.78(3) \cdot 10^{-2}$ between coherent ($e_U = 0.37(3) \cdot 10^{-2}$) and stochastic ($e_S = 1.41(1) \cdot 10^{-2}$) error types. The dominant source of error in the gate is stochastic error. We es-

timate the decoherence-limited Clifford process infidelity $e_{\text{decoh.}}$ using the measured T_1 and T_2^{echo} for Q_c (Q_t) of $T_1 = 65(5)\,\mu$s ($T_1 = 58(9)\,\mu$s) and $T_2^{\text{echo}} = 86(6)\,\mu$s, ($T_2^{\text{echo}} = 77(8)\,\mu$s), and the average Clifford gate length of 389 ns, which gives $e_{\text{decoh.}} = 0.76 \cdot 10^{-2}$. The larger observed e_S than the $e_{\text{decoh.}}$ suggests that other forms of stochastic error are present beyond those introduced by relaxation and dephasing of the qubit transition levels. This could be due to decoherence channels of higher transmon levels participating in the interaction via state hybridization between computational and noncomputational levels during the drive [27]. We measured reduced coherence when applying the CZ drive, described in the supplementary material. To summarize, we measure the CZ gate fidelity to be 99.43(1)%, with low leakage and the dominant source of remaining errors being stochastic error. The discrepancy between stochastic error and predicted error from decoherence suggests additional sources of stochastic error are present during the gate.

We have demonstrated a tunable ZZ interaction between fixed frequency, fixed coupling transmons using off-resonant, simultaneous charge drives. This tunable ZZ coupling enables both cancellation and enhancement of the static ZZ interaction. We implemented a high fidelity CZ gate that is resilient against drive crosstalk and static ZZ interactions during the gate. We expect with this interaction one can leverage higher exchange coupling J between qubits to further reduce CZ gate times, and multi-path couplers that suppress static ZZ [18] can be combined with this drive to eliminate the unwanted ZZ during idling [7] or during operation of other gates. Further, the off-resonant character of the interaction provides drive frequency flexibility, reducing frequency crowding constraints with scaling up fixed frequency, fixed coupling quantum processors. Quantifying multi-qubit errors of this gate on a larger quantum processor, including spectator errors and simultaneous gate operation with spectator ZZ cancellation, is a subject of future work. While we utilize this charge-activated tunable ZZ interaction to implement a CZ gate, it can also be applied to simulation of exotic quantum many-body physics, including the extended Bose-Hubbard model [48–51] and nonreciprocal interacting photonic systems [52, 53], as well as realizing native quantum stabilizer measurements [54], without the need for additional flux-based tunable components.

We thank Larry Chen, Trevor Chistolini, William Livingston, Dr. Long Nguyen, and Dr. Jean-Loup Ville for valuable discussions. This material is based upon work supported in part by the U.S. Army Research Laboratory and the U.S. Army Research Office under contract/grant number W911NF-17-S-0008 and the National Defense Science & Engineering Graduate (NDSEG) Fellowship.

[1] M. Kjaergaard, M. E. Schwartz, J. Braumüller, P. Krantz, J. I.-J. Wang, S. Gustavsson, and W. D. Oliver, Annual Review of Condensed Matter Physics **11**, 369 (2020).

[2] J. Ghosh, A. G. Fowler, J. M. Martinis, and M. R. Geller, Physical Review A **88**, 062329 (2013).

[3] A. Blais, R.-S. Huang, A. Wallraff, S. M. Girvin, and R. J. Schoelkopf, Physical Review A , 14 (2004).

[4] A. G. Fowler, M. Mariantoni, J. M. Martinis, and A. N. Cleland, Physical Review A **86**, 032324 (2012).

[5] M. C. Collodo, J. Herrmann, N. Lacroix, C. K. Andersen, A. Remm, S. Lazar, J.-C. Besse, T. Walter, A. Wallraff, and C. Eichler, Physical Review Letters **125**, 240502 (2020).

[6] Y. Xu, J. Chu, J. Yuan, J. Qiu, Y. Zhou, L. Zhang, X. Tan, Y. Yu, S. Liu, J. Li, F. Yan, and D. Yu, Physical Review Letters **125**, 240503 (2020).

[7] P. Mundada, G. Zhang, T. Hazard, and A. Houck, Physical Review Applied **12**, 054023 (2019).

[8] V. Negîrneac, H. Ali, N. Muthusubramanian, F. Battistel, R. Sagastizabal, M. S. Moreira, J. F. Marques, W. Vlothuizen, M. Beekman, N. Haider, A. Bruno, and L. DiCarlo, arXiv:2008.07411 [quant-ph] (2020), arXiv: 2008.07411.

[9] J. Stehlik, D. M. Zajac, D. L. Underwood, T. Phung, J. Blair, S. Carnevale, D. Klaus, G. A. Keefe, A. Carniol, M. Kumph, M. Steffen, and O. E. Dial, arXiv:2101.07746 [quant-ph] (2021), arXiv: 2101.07746.

[10] Y. Sung, L. Ding, J. Braumüller, A. Vepsäläinen, B. Kannan, M. Kjaergaard, A. Greene, G. O. Samach, C. McNally, D. Kim, A. Melville, B. M. Niedzielski, M. E. Schwartz, J. L. Yoder, T. P. Orlando, S. Gustavsson, and W. D. Oliver, arXiv:2011.01261 [quant-ph] (2020).

[11] G. S. Paraoanu, Physical Review B **74**, 140504 (2006).

[12] J. M. Chow, J. M. Gambetta, A. W. Cross, S. T. Merkel, C. Rigetti, and M. Steffen, New Journal of Physics **15**, 115012 (2013).

[13] S. Puri and A. Blais, Physical Review Letters **116**, 180501 (2016).

[14] H. Paik, A. Mezzacapo, M. Sandberg, D. McClure, B. Abdo, A. Córcoles, O. Dial, D. Bogorin, B. Plourde, M. Steffen, A. Cross, J. Gambetta, and J. M. Chow, Physical Review Letters **117**, 250502 (2016).

[15] C. Rigetti and M. Devoret, Physical Review B **81**, 134507 (2010).

[16] J. Long, T. Zhao, M. Bal, R. Zhao, G. S. Barron, H.-s. Ku, J. A. Howard, X. Wu, C. R. H. McRae, X.-H. Deng, G. J. Ribeill, M. Singh, T. A. Ohki, E. Barnes, S. E. Economou, and D. P. Pappas, arXiv:2103.12305 [quant-ph] (2021), arXiv: 2103.12305.

[17] S. Krinner, P. Kurpiers, B. Royer, P. Magnard, I. Tsitsilin, A. Blais, and A. Wallraff, Physical Review Applied , 11 (2020).

[18] A. Kandala, K. X. Wei, S. Srinivasan, E. Magesan, S. Carnevale, G. A. Keefe, D. Klaus, O. Dial, and D. C. McKay, arXiv:2011.07050 [quant-ph] (2020), arXiv: 2011.07050.

[19] L. DiCarlo, J. M. Chow, J. M. Gambetta, L. S. Bishop, B. R. Johnson, D. I. Schuster, J. Majer, A. Blais, L. Frunzio, S. M. Girvin, and R. J. Schoelkopf, Nature **460**, 240 (2009).

[20] J. M. Gambetta, A. D. Corcoles, S. T. Merkel, B. R. Johnson, J. A. Smolin, J. M. Chow, C. A. Ryan, C. Rigetti, S. Poletto, T. A. Ohki, M. B. Ketchen, and M. Steffen, Physical Review Letters **109**, 240504 (2012), arXiv: 1204.6308.

[21] D. C. McKay, S. Sheldon, J. A. Smolin, J. M. Chow, and J. M. Gambetta, Physical Review Letters **122**, 200502 (2019).

[22] A. Morvan, V. V. Ramasesh, M. S. Blok, J. M. Kreikebaum, K. O'Brien, L. Chen, B. K. Mitchell, R. K. Naik, D. I. Santiago, and I. Siddiqi, arXiv:2008.09134 [quant-ph] (2020), arXiv: 2008.09134.

[23] S. Krinner, S. Lazar, A. Remm, C. Andersen, N. Lacroix, G. Norris, C. Hellings, M. Gabureac, C. Eichler, and A. Wallraff, Physical Review Applied **14**, 024042 (2020).

[24] S. Sheldon, E. Magesan, J. M. Chow, and J. M. Gambetta, Physical Review A **93**, 060302 (2016).

[25] N. Sundaresan, I. Lauer, E. Pritchett, E. Magesan, P. Jurcevic, and J. M. Gambetta, PRX Quantum **1**, 020318 (2020).

[26] J. Ku, X. Xu, M. Brink, D. C. McKay, J. B. Hertzberg, M. H. Ansari, and B. Plourde, Physical Review Letters **125**, 200504 (2020).

[27] H. Xiong, Q. Ficheux, A. Somoroff, L. B. Nguyen, E. Dogan, D. Rosenstock, C. Wang, K. N. Nesterov, M. G. Vavilov, and V. E. Manucharyan, arXiv:2103.04491 [cond-mat, physics:quant-ph] (2021), arXiv: 2103.04491.

[28] J. Koch, T. M. Yu, J. Gambetta, A. A. Houck, D. I. Schuster, J. Majer, A. Blais, M. H. Devoret, S. M. Girvin, and R. J. Schoelkopf, Physical Review A **76**, 042319 (2007).

[29] J. B. Hertzberg, E. J. Zhang, S. Rosenblatt, E. Magesan, J. A. Smolin, J.-B. Yau, V. P. Adiga, M. Sandberg, M. Brink, J. M. Chow, and J. S. Orcutt, arXiv:2009.00781 [cond-mat, physics:quant-ph] (2020), arXiv: 2009.00781.

[30] E. J. Zhang, S. Srinivasan, N. Sundaresan, D. F. Bogorin, Y. Martin, J. B. Hertzberg, J. Timmerwilke, E. J. Pritchett, J.-B. Yau, C. Wang, W. Landers, E. P. Lewandowski, A. Narasgond, S. Rosenblatt, G. A. Keefe, I. Lauer, M. B. Rothwell, D. T. McClure, O. E. Dial, J. S. Orcutt, M. Brink, and J. M. Chow, arXiv:2012.08475 [quant-ph] (2020), arXiv: 2012.08475.

[31] J. Preskill, Quantum **2**, 79 (2018), arXiv: 1801.00862.

[32] N. Lacroix, C. Hellings, C. K. Andersen, A. Di Paolo, A. Remm, S. Lazar, S. Krinner, G. J. Norris, M. Gabureac, J. Heinsoo, A. Blais, C. Eichler, and A. Wallraff, PRX Quantum **1**, 110304 (2020).

[33] B. Foxen, C. Neill, A. Dunsworth, P. Roushan, B. Chiaro, A. Megrant, J. Kelly, Z. Chen, K. Satzinger, R. Barends, F. Arute, K. Arya, R. Babbush, D. Bacon, J. Bardin, S. Boixo, D. Buell, B. Burkett, Y. Chen, R. Collins, E. Farhi, A. Fowler, C. Gidney, M. Giustina, R. Graff, M. Harrigan, T. Huang, S. Isakov, E. Jeffrey, Z. Jiang, D. Kafri, K. Kechedzhi, P. Klimov, A. Korotkov, F. Kostritsa, D. Landhuis, E. Lucero, J. McClean, M. McEwen, X. Mi, M. Mohseni, J. Mutus, O. Naaman, M. Neeley, M. Niu, A. Petukhov, C. Quintana, N. Rubin, D. Sank, V. Smelyanskiy, A. Vainsencher, T. White, Z. Yao, P. Yeh, A. Zalcman, H. Neven, J. Martinis, and Google AI Quantum, Physical Review Letters **125**,

120504 (2020).
[34] V. Tripathi, M. Khezri, and A. N. Korotkov, Physical Review A **100** (2019), 10.1103/PhysRevA.100.012301.
[35] N. F. Ramsey, Physical Review **78**, 695 (1950).
[36] M. S. Blok, V. V. Ramasesh, T. Schuster, K. O'Brien, J. M. Kreikebaum, D. Dahlen, A. Morvan, B. Yoshida, N. Y. Yao, and I. Siddiqi, Phys. Rev. X **11**, 021010 (2021).
[37] D. C. McKay, C. J. Wood, S. Sheldon, J. M. Chow, and J. M. Gambetta, Physical Review A **96**, 022330 (2017).
[38] J. Emerson, R. Alicki, and K. Życzkowski, Journal of Optics B: Quantum and Semiclassical Optics **7**, S347 (2005).
[39] E. Knill, D. Leibfried, R. Reichle, J. Britton, R. B. Blakestad, J. D. Jost, C. Langer, R. Ozeri, S. Seidelin, and D. J. Wineland, Physical Review A , 7 (2008).
[40] E. Magesan, J. M. Gambetta, B. R. Johnson, C. A. Ryan, J. M. Chow, S. T. Merkel, M. P. da Silva, G. A. Keefe, M. B. Rothwell, T. A. Ohki, M. B. Ketchen, and M. Steffen, Physical Review Letters **109** (2012), 10.1103/PhysRevLett.109.080505.
[41] R. Harper, Physical Review A , 7 (2019).
[42] A. Carignan-Dugas, J. J. Wallman, and J. Emerson, New Journal of Physics **21**, 053016 (2019).
[43] A. Erhard, J. J. Wallman, L. Postler, M. Meth, R. Stricker, E. A. Martinez, P. Schindler, T. Monz, J. Emerson, and R. Blatt, Nature Communications **10**, 5347 (2019).
[44] C. J. Wood and J. M. Gambetta, Physical Review A **97**, 032306 (2018).
[45] Z. Chen, J. Kelly, C. Quintana, R. Barends, B. Campbell, Y. Chen, B. Chiaro, A. Dunsworth, A. Fowler, E. Lucero, E. Jeffrey, A. Megrant, J. Mutus, M. Neeley, C. Neill, P. O'Malley, P. Roushan, D. Sank, A. Vainsencher, J. Wenner, T. White, A. Korotkov, and J. M. Martinis, Physical Review Letters **116**, 020501 (2016).
[46] J. Wallman, C. Granade, R. Harper, and S. T. Flammia, New Journal of Physics **17**, 113020 (2015).
[47] S. J. Beale, A. Carignan-Dugas, D. Dahlen, J. Emerson, I. Hincks, P. Iyer, A. Jain, D. Hufnagel, E. Ospadov, J. Saunders, A. Stasiuk, J. J. Wallman, and A. Winick, "True-Q," (2020).
[48] M. Kounalakis, C. Dickel, A. Bruno, N. K. Langford, and G. A. Steele, npj Quantum Information **4**, 38 (2018).
[49] P. Roushan, C. Neill, J. Tangpanitanon, V. M. Bastidas, A. Megrant, R. Barends, Y. Chen, Z. Chen, B. Chiaro, A. Dunsworth, A. Fowler, B. Foxen, M. Giustina, E. Jeffrey, J. Kelly, E. Lucero, J. Mutus, M. Neeley, C. Quintana, D. Sank, A. Vainsencher, J. Wenner, T. White, H. Neven, D. G. Angelakis, and J. Martinis, Science **358**, 1175 (2017).
[50] Y. Ye, Z.-Y. Ge, Y. Wu, S. Wang, M. Gong, Y.-R. Zhang, Q. Zhu, R. Yang, S. Li, F. Liang, J. Lin, Y. Xu, C. Guo, L. Sun, C. Cheng, N. Ma, Z. Y. Meng, H. Deng, H. Rong, C.-Y. Lu, C.-Z. Peng, H. Fan, X. Zhu, and J.-W. Pan, Physical Review Letters **123**, 050502 (2019).
[51] J. Jin, D. Rossini, R. Fazio, M. Leib, and M. J. Hartmann, Physical Review Letters **110**, 163605 (2013).
[52] P. Roushan, C. Neill, A. Megrant, Y. Chen, R. Babbush, R. Barends, B. Campbell, Z. Chen, B. Chiaro, A. Dunsworth, A. Fowler, E. Jeffrey, J. Kelly, E. Lucero, J. Mutus, P. J. J. O'Malley, M. Neeley, C. Quintana, D. Sank, A. Vainsencher, J. Wenner, T. White, E. Kapit, H. Neven, and J. Martinis, Nature Physics **13**, 146 (2017).
[53] X. Guan, Y. Feng, Z.-Y. Xue, G. Chen, and S. Jia, Physical Review A **102**, 032610 (2020).
[54] C. K. Andersen, A. Remm, S. Lazar, S. Krinner, N. Lacroix, G. J. Norris, M. Gabureac, C. Eichler, and A. Wallraff, Nature Physics **16**, 875 (2020).